Micro- and nano-characterization of Zn-clays in nonsulfide supergene ores of southern Peru

Nicola Mondillo[1,*], Fernando Nieto[2] and Giuseppina Balassone[1]

[1]Dipartimento di Scienze della Terra, dell'Ambiente e delle Risorse, Università degli Studi di Napoli Federico II, Via Mezzocannone, 8 I-80134 Napoli Italy
[2]Departamento de Mineralogía y Petrología and IACT, Universidad de Granada, CSIC, Av. Fuentenueva, 18002 Granada, Spain

Abstract

Zn-clays are associated with several supergene nonsulfide ore deposits worldwide, where they are either the prevailing economic minerals, or minor components of the weathering-derived mineral assemblage. A TEM-HRTEM study on Zn-clays from nonsulfide ore deposits of Accha and Yanque (Peru) was carried out, to properly determine the chemistry and complex texture of these clays, not fully defined in other previous works on these (but also on other similar) deposits. The Zn-clays occurring at Accha and Yanque are constituted by a mixture of sauconite and Zn-bearing beidellite. The chemical composition of sauconite varies in a range of values, without any chemical gap, around the average composition:

$$Ca_{0.15}K_{0.05}(Zn_{2.1}Mg_{0.2}Al_{0.4}Fe_{0.15}Mn_{0.02})(Si_{3.5}Al_{0.5})O_{10}(OH)_2 \cdot nH_2O.$$

Beidellites present an average composition close to stoichiometry with the addition of Zn:

$$Ca_{0.05}K_{0.15}(Al_{1.6}Zn_{0.25}Mg_{0.1}Fe_{0.15})(Si_{3.6}Al_{0.4})O_{10}(OH)_2 \cdot nH_2O.$$
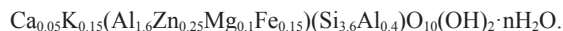
The chemical composition of both sauconite and beidellite is consistent through the samples, with sauconite affected by a wider variation in composition than beidellite. The textures of Zn-bearing smectites clearly indicate that a part of these clays grew on precursory mica-like phyllosilicates, whereas another part was derived from a direct precipitation from solutions. The occurrence of a paragenesis with trioctahedral and dioctahedral smectites demonstrates that, as observed in other environments, also in a Zn-bearing system both smectite types are stable. As proved for other analogous trioctahedral-dioctahedral smectite systems (e.g., saponite-beidellite), also in the sauconite-beidellite system a chemical compositional gap exists within the series. The texture indicating a direct precipitation from solutions does not exclude that a smectite amount could be genetically related to hydrothermal fluids, even if several other characteristics (e.g., the paragenetical association with Fe-hydroxides typical of gossans) confirm the supergene origin for the bulk of the deposit.

Keywords: Sauconite, Zn-beidellite, nonsulfide zinc ore deposits, TEM-HRTEM

Introduction

Zn-bearing clay minerals occur in several nonsulfide zinc ores (Hitzman et al. 2003; Large 2001). Zinc nonsulfide deposits are concentrations of economic Zn-oxidized minerals, mainly represented by smithsonite, hydrozincite, hemimorphite, sauconite, and willemite, markedly different from sphalerite ores, typically exploited for zinc (Hitzman et al. 2003; Large 2001). Nonsulfide ores are genetically related to supergene or hypogene processes: the supergene deposits primarily form from the oxidation of sulfide-bearing concentrations in a weathering regime, whereas the hypogene deposits form after mineral precipitation from hydrothermal or metamorphic fluids (Hitzman et al. 2003).

Zn-clays are worldwide associated with several supergene nonsulfide ores, where they are either the prevailing economic minerals or minor components of the weathering-derived mineral assemblage (Balassone et al. 2008; Boland et al. 2003; Boni et al. 2009; Borg et al. 2003; Coppola et al. 2008; Emselle et al. 2005; Frondel 1972; Ahn 2010; Kärner 2006). The best example is the world-class Skorpion mineralization (Namibia)—the largest supergene nonsulfide zinc deposit in the world (original reserves of 24.6 Mt ore at 10.6% Zn)—where sauconite, the trioctahedral Zn-bearing smectite (Newman and Brown 1987; Ross 1946), predominates over the other Zn-oxidized minerals (Borg et al. 2003; Kärner 2006).

Herein we present the first combined TEM-AEM and HRTEM crystal-chemical characterization of natural Zn-clay minerals, associated with two nonsulfide ore deposits in Peru (Yanque and Accha). In fact, TEM is pivotal for the characterization of crystalline materials at nano- and sub-nanometer scale, such as clays (Nieto and Livi 2013), allowing for a wide range of imaging and diffraction techniques. When coupled with AEM analytical tools,
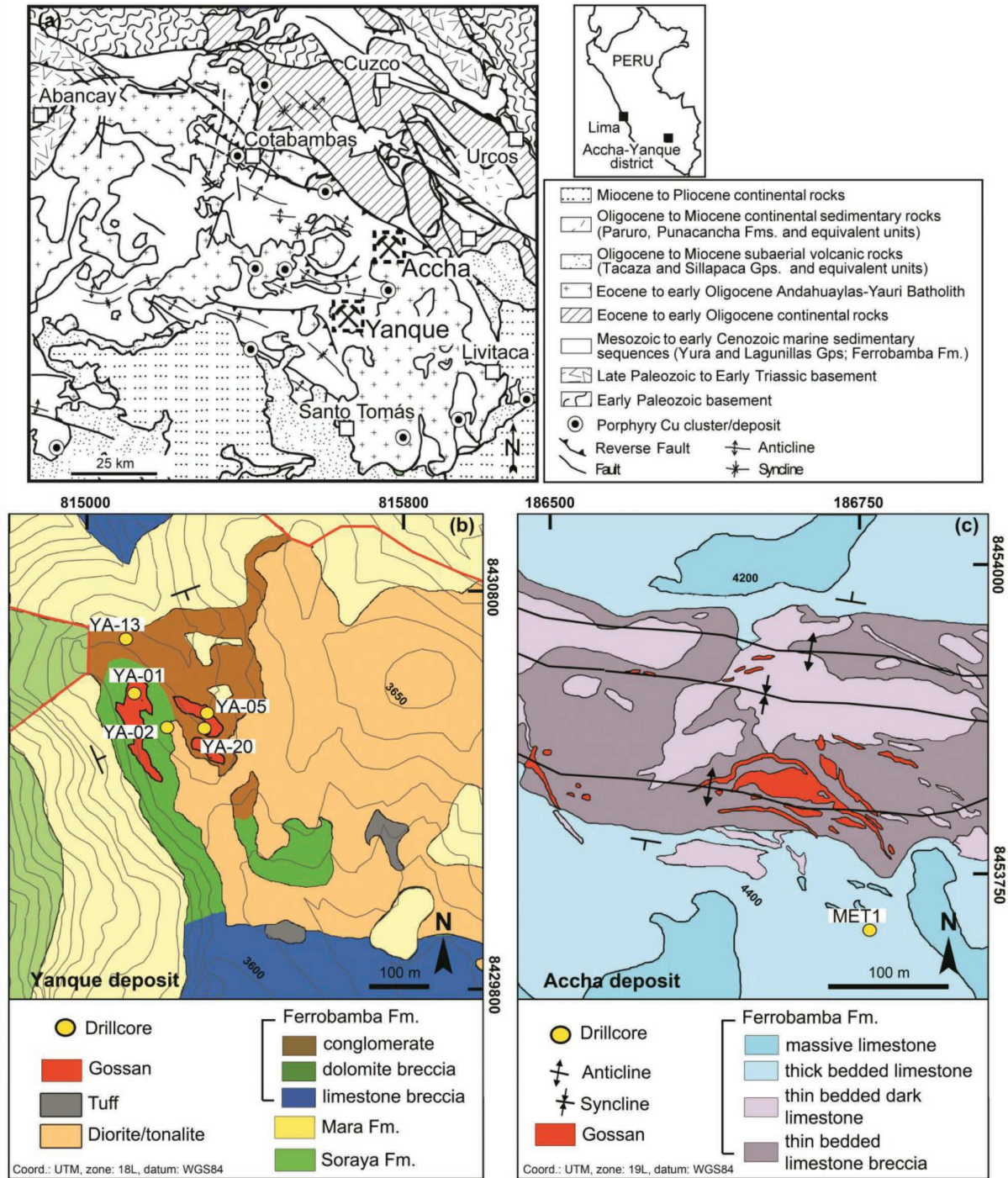
---

* E-mail: nicola.mondillo@unina.it

FIGURE 1. (**a**) General geologic map of the Andahuaylas-Yauri metallogenic province (modified from Perelló et al. 2003). (**b**) Geologic map of the Yanque deposit area (modified from Mondillo et al. 2014a). (**c**) Geologic map of the Accha deposit area (modified from Boni et al. 2009).

TABLE 1. Zn-bearing clay minerals and other phyllosilicates

Name	Ideal formula[a]
Baileychlore	$(Zn,Fe^{2+},Al,Mg)_6(Si,Al)_4O_{10}(OH)_8$
Bannisterite	$KCa(Mn^{2+},Fe^{2+},Zn,Mg)_{20}(Si,Al)_{32}O_{76}(OH)_{16}\cdot4–12H_2O$
Fraipontite	$(Zn,Al)_3(Si,Al)_2O_5(OH)_4$
Franklinfurnaceite	$Ca_2(Fe^{3+},Al)Mn^{3+}Mn_2^{2+}Zn_2Si_2O_{10}(OH)_8$
Hendricksite	$K(Zn,Mg,Mn^{2+})_3(Si_3Al)O_{10}(OH)_2$
Sauconite	$Na_{0.3}Zn_3(Si,Al)_4O_{10}(OH)_2\cdot4H_2O$
[a] IMA accepted.	

elemental composition and atomic structure down to a single atom can be provided as well. The aim of this work is to determine chemistry and textures of the Zn-clays occurring in the Yanque and Accha deposits. These characteristics can be important when planning a correct metallurgical processing, but also, being strictly related to environmental conditions during mineral formation, allow to better constrain the genesis of the ore deposits.

TABLE 2. XRD semi-quantitative analyses of Yanque and Accha samples selected for TEM study, after Boni et al. (2009) and Mondillo et al. (2014)

Drillcore	Latitude (Y)[a]	Longitude (X)[a]	Drillhole elevation (m.s.l.)	Sample depth from the top of the core (m)	Sample name	Hemimorphite	Smithsonite	Zn-smectite
YA-01	8430548	815103	3562	1.5	YA-A	O	OO	OOO
YA-02	8430449	815202	3566	5.0	YA-B	OOO	–	OOO
YA-05	8430484	815297	3549	8.5	YA-C	OO	–	OOO
YA-13	8430673	815099	3544	9.0	YA-D	OO	–	OOO
YA-20	8430461	815295	3553	9.0	YA-E	–	–	OOOO
MET1-26	8453672	186758	4287	98.5	ACC	–	O	OOOO

[a] Coordinates: UTM, zone: 18L (Yanque) and 19L (Accha), datum: WGS84; – = not found, O <5 wt%, OO 5–20 wt%, OOO 20–40 wt%, OOOO 40–60 wt%.

(Table extends on next page)

AN OVERVIEW ON Zn-BEARING PHYLLOSILICATES

A list of Zn-bearing clay minerals and other phyllosilicates is given in Table 1. Sauconite is the predominant Zn-bearing clay in zinciferous nonsulfide ore deposits (Boni 2005; Hitzman et al. 2003). It was recognized for the first time in the Uberroth Mine, near Friendensville, in the Saucon Valley of Pennsylvania (Genth 1875). The validity of the species was later proved by Ross (1946), who also produced the chemical formula still accepted by the International Mineralogical Association (IMA). Sauconite has a saponite-like structure, with a tetrahedral charge related to Al/Si substitutions in tetrahedral sheets (Faust 1951; Ross 1946), while Zn takes the place of Mg in the octahedral positions.

Several experimental studies on the synthesis and stability of sauconite were carried out (Harder 1977; Higashi et al. 2002; Kloprogge et al. 1999; Pascua et al. 2010; Petit et al. 2008; Roy and Mumpton 1956; Tiller and Pickering 1974). These studies demonstrated that Zn-smectite can precipitate from solutions of silicic acid, variously mixed with Zn-compounds (Zn-chloride, Zn-oxide, or Zn-hydroxide), Na-compounds, and Al-compounds, at temperatures ranging between 20 and 200 °C for pH from 6 to 12. The retention of base (Zn) and heavy metals in other phyllosilicate lattices through adsorption mechanisms, as in kaolinite, has been also investigated (Gu and Evans 2008; Miranda-Trevino and Coles 2003; Srivastava et al. 2005).

Several occurrences of sauconite have been reported worldwide, e.g., in the Moresnet-Altenberg nonsulfide deposit (La Calamine) in Belgium (Coppola et al. 2008; Frondel 1972), in the supergene weathering zones of the Irish Tynagh and Silvermines deposits (Balassone et al. 2008), in the Shaimerden deposit, Kazakhstan (Boland et al. 2003), in the Sierra Mojada Zn district in Mexico (Ahn 2010), and in the Reliance deposit near Beltana, South Australia (Emselle et al. 2005; Hitzman et al. 2003). In these deposits, sauconite is associated with smithsonite and hemimorphite, and is considered a product of the weathering of Zn-bearing sulfides. In the Skorpion zinc deposit (Namibia), sauconite mainly occurs as coatings of intergranular spaces and voids; it formed after the breakdown and dissolution of feldspars and micas (Borg et al. 2003; Kärner 2006).

All the other Zn-bearing phyllosilicates have been generally considered as rare species in natural Zn-oxidized deposits (Hitzman et al. 2003).

Fraipontite, a Zn-bearing clay belonging to the kaolinite-serpentine group, was first described by Cesàro (1927), who found a "*silicate double de zinc et d'aluminum hydrate*" in the Vieille-Montagne Mine (Belgium). The mineral was definitely validated by Fransolet and Bourguignon (1975), who carried out a structural characterization of the original specimen and also proposed the chemical formula actually accepted by IMA.

Fraipontite is considered a weathering-related clay mineral, as, for example, in the Belgian deposits (Coppola et al. 2008), or also associated with low-temperature hydrothermal fluids, as in Preguiça mine, Southern Portugal (Will et al. 2014).

Baileychlore, the Zn-bearing end-member of the trioctahedral chlorite series, was recognized and validated by Rule and Radke (1988) in a specimen from the Red Dome deposit, North Queensland (Australia).

A Zn-phyllosilicate intermediate between chlorite and mica is the franklinfurnaceite (Peacor et al. 1988), which was solely recognized in association with willemite in the Franklin mine, New Jersey (U.S.A.).

Up to date, in clearly hydrothermal/metamorphic deposits in the U.S.A. (e.g., Franklin, New Jersey) and Australia (Broken Hill), two types of Zn-mica have been identified, i.e., bannisterite (Heaney et al. 1992) and hendricksite (Robert and Gaspérin 1985).

BACKGROUND INFORMATION ON PERUVIAN Zn CLAY-BEARING DEPOSITS

Geological setting

The present study is based on the Zn-smectites from the Yanque and Accha nonsulfide Zn-Pb deposits, Cuzco region, in southern Peru (Boni et al. 2009; Mondillo et al. 2014a).

The Yanque and Accha deposits are located in the Andahuaylas-Yauri metallogenic province, extending for several hundred square kilometers around the town of Cuzco. The Andahuaylas-Yauri province hosts numerous porphyry copper and porphyry-related skarn deposits that are spatially and temporally associated with the middle Eocene to early Oligocene (ca. 48–32 Ma) intrusions of the Andahuaylas-Yauri batholith into Mesozoic sediments (Fig. 1a) (Perelló et al. 2003). The Accha-Yanque Belt covers a wide area located in the middle of the Andahuaylas province; it hosts many Zn and Pb ores, as well as several porphyry copper deposits of variable sizes.

The Yanque prospect is a Zn-Pb nonsulfide concentration located 20 km north of Santo Tomás village. The orebody covers an approximate surface area of 900 × 500 m, and contains 26 491 kilotonnes of indicated resources at 2.37% Zn and 2.18% Pb (1.67% ZnEq cutoff) (Zincore Metals, Inc. 2013). The deposit consists of several sub-horizontal stratabound bodies that extend in depth to more than 100 m. Yanque is hosted by a sedimentary breccia with lateral facies variations, which stratigraphically comprehends parts of the Mara and Ferrobamba Formations (Pecho and Blanco 1983) (Fig. 1b). The mineralized breccia consists of a siliciclastic conglomerate, heteropic to a breccia containing dolomite clasts. The emplacement of the original

TABLE 2.—EXTENDED

Drillcore	Chalcophanite	Cerussite	Quartz	K-Feldspar	Calcite	Dolomite	Illite	Kaolinite	Goethite
YA-01	–	–	OO	–	OO	OO	OO	O	O
YA-02	–	–	OO	–	–	–	–	O	OO
YA-05	–	–	OOO	O	–	–	–	OO	–
YA-13	–	OO	OO	O	–	–	O	–	O
YA-20	O	–	OOO	O	–	–	–	O	–
MET1-26	OOO	–	OOO	–	–	–	–	O	–

sulfide mineralization produced a phyllic alteration of the sedimentary breccia, characterized by alteration of feldspars and precipitation of microcrystalline mica (Mondillo et al. 2014a).

The Accha deposit is a sphalerite mineralization hosted in Mesozoic rocks, almost fully oxidized to smithsonite. The mineralized zone [6613 kilotonnes of measured and indicated resources at 6.37% Zn and 0.78% Pb (2.20% ZnEq cutoff) (Zincore Metals, Inc. 2013)] occupies the hinge of an anticlinal dome that has been exposed by erosion. The nonsulfide concentrations, consisting of a mineralized zone 5 to 20 m thick, are continuous along strike to the west for at least 700 m (Boni et al. 2009).

The main host to mineralization consists of carbonate-clay matrix-supported breccias and locally by very thin, quartz-rich conglomerate layers (Fig. 1c). The total thickness of the brecciated interval, visible both in outcrop and in drill core, varies from 50 to 100 m, whereas individual breccia zones are continuous over 5 to 20 m downhole (Boni et al. 2009).

Both Yanque and Accha nonsulfide deposits formed after the oxidation of original sulfide protores, which, together with several Cu-porphyry deposits, are genetically related to the emplacement of the Andahuaylas-Yauri batholith (Boni et al. 2009; Mondillo et al. 2014a, 2014b).

Mineralogy and petrography of Yanque and Accha ores

Sauconite is the most abundant economic Zn mineral in the Yanque deposit (Mondillo et al. 2014a). It was observed in association with a Zn-bearing mica (indicated as Zn-illite by the above authors) with Zn in its octahedral site, and with a Zn-bearing kaolinite, where Zn was considered not to be a cation in the clay structure, but an element adsorbed by the Fe-hydroxides associated with clays (Mondillo et al. 2014a). Sauconite in the Yanque deposit was considered to have been mainly formed through replacement of K-feldspar and muscovite of the host rock by weathering process. Other components of the Yanque mineralization are hemimorphite, smithsonite, cerussite, and secondary silver sulfides (i.e., acanthite). The original primary sulfides are virtually lacking in the deposit.

The Accha nonsulfide mineral association consists mainly of smithsonite and hemimorphite replacing both primary ore minerals and carbonate host rocks. Sauconite is less abundant, but it has been detected throughout the deposit with the more abundant smithsonite and hemimorphite. According to Boni et al. (2009) sauconite is genetically related to supergene transformation of the potassic alumosilicates, and/or forms the filling of the remaining porosity of the host rock.

X-ray diffraction analyses were carried out on clay separates of Yanque samples by Mondillo et al. (2014a) under different conditions. X-ray diffraction patterns of the air-dried, ethylene glycol solvated, and heated (550 °C) clay aggregates resulted to be typical of expandable smectites, here identified as sauconite (Table 2). These analyses excluded the occurrence in the Yanque deposit of Zn-bearing phyllosilicates of the chlorite group (e.g., baileychlore), which have almost the same air-dried pattern of sauconite, but are characterized by non-expandable characteristics.

MATERIALS

For TEM-AEM analyses, we have selected five samples from the Yanque deposit and one sample from the Accha deposit, by using drillcore sections having medium-high Zn-grade and moderate/high clay contents, already analyzed by Boni et al. (2009) and Mondillo et al. (2014a). Their mineral assemblages, inferred by semi-quantitative mineralogical X-ray diffraction, are reported in Table 2.

Yanque samples are characterized by abundant phyllosilicates, in particular sauconite, illite, and kaolinite (Table 2). Samples YA-D and YA-E originate from some deeply altered parts of the siliciclastic conglomerate, which hosts the Yanque Zn-Pb mineralization, whereas samples YA-A, YA-B, and YA-C were collected from sandstone-shale lenses within the conglomerate.

Sample ACC was collected in the Accha deposit from a mineralized quartz-rich conglomerate layer with abundant sauconite, interlayered within the limestone containing the main smithsonite orebody. This sample mostly consists of detrital quartz, Zn-Mn-hydroxides (mostly chalcophanite), and sauconite (Table 2).

METHOD

The particle morphology and quantitative chemical analyses were obtained using TEM and AEM, respectively. The microscope used was a Philips CM20, at the C.I.C. of the University of Granada, operating at 200 kV, with an EDAX solid-state EDX detector. Lifetime of analyses was 100 s; areas producing dead time higher than 5% were rejected to ensure the thin character required by the Cliff and Lorimer (1975) approximation. Analyses were obtained, using STEM mode, from powdered portions deposited on a holey C-coated Au grid. This mode of preparation disperses individual grains of minerals onto the grid surface. Albite, biotite, muscovite, spessartine, olivine, titanite, and hemimorphite standards were measured using the same protocol as samples, to obtain K-factors for the transformation of intensity ratios to concentration ratios according to Cliff and Lorimer (1975). The structural formulas of smectite and mica were calculated on the basis of 22 negative charges, i.e., $O_{10}(OH)_2$. According to the accepted stoichiometry of smectites (Güven 1988), Fe was considered as bivalent for trioctahedral species (e.g., sauconite), and trivalent for dioctahedral species (e.g., beidellite). The Na content in the Zn-clays was not measured, because of the Na-Zn peaks overlap in the energy-dispersion spectrum. However, as reported by Mondillo et al. (2014a), ICP-MS analyses on a clay-rich fraction excluded the occurrence of significant amounts of Na in these minerals, where a maximum content of about 0.5% of this element has been detected.

Two samples (YA-B and YA-D) were also analyzed in HRTEM mode on thin sections, to investigate the microscopic texture of clays. The samples were chosen considering their different clay association detected at TEM-AEM. Copper rings were attached to representative selected areas of the matrix of thin sections prepared with Canada balsam and after ion-thinned, using a Fischione Model 1050 ion mill, and carbon coated. Ion milling was performed at 4 kV and ±10°, until the first hole and ±7° during 20 min for final cleaning. The HRTEM study was performed at the CIC of the University of Granada (Spain) using a Titan TEM with XFEG emission gun, spherical aberration corrector and HAADF detector, working at 300 kV, with

a resolution of 0.8 Å in the TEM mode and 2 Å in the STEM mode. EDX spectra for qualitative identification of minerals and chemical maps were obtained using the Super-X system.

<div align="center">RESULTS</div>

Texture of clays

The texture of the Zn-clays was observed in the samples YA-B and YA-D, whose preparation using ion-milling technique provided the preservation of the mineral fabric (Figs. 2 and 3). At low magnification, the two samples present similar characteristics, and they generally produce comparable electron diffraction patterns (SAED). Therefore they will be described together.

At a size below 10 μm, smectite forms two types of microtextures here indicated as "compact clay packages" (CCP) and "porous clay aggregates" (PCA) (Figs. 2a and 2b).

CCP (Fig. 2a) are characterized by nearly isoriented clay packets. This microtexture can have a length up to several micrometers and a thickness below 1 μm, and the packets can be straight or slightly curved. In the packets, the clay layers can be curved and show a wavy microfabric. In the CCP, smectite grains can overgrow upon mica nuclei, forming a sort of epitaxial structure (Figs. 2c and 2d). Compact smectite packets produce electron diffraction patterns constituted by the superposition of concentric circles, characteristic of a powder-type diagram, and oblique trends of points, corresponding to various individual crystals partly disoriented between each other (Fig. 4). Both the powder circles and mono-crystals have a 10 Å spacing, which indicates the typical collapse of smectitic layers related to the microscope vacuum. Figure 4b shows the electron diffraction pattern of the smectite packet shown on Figures 2c and 2d, epitaxial over a mica grain; both smectite and mica present a 10 Å basal spacing, but they can be easily distinguished by their different crystallinity. Mica electron diffraction pattern shows also some general rows having a spacing of 20 Å, which allows the identification of mica 2*M* polytype.

The PCA are characterized by random orientation of the clay packets, which typically show a very fine grain size, lower than those detected in CCP (Fig. 2b). The random orientation produces radial to dendritic microtextures and leaves spaces between the grains. The voids of these aggregates are frequently occupied by Fe-hydroxides (Figs. 2e, 2f, and 3), which can have a spongy texture (Fig. 2e), or also occur as rhombic micro-grains and radial aggregates of oblong crystals (Fig. 2f). Electron diffraction patterns of PCA show that smectite has a turbostratic arrangement. When the porous packets are associated with Fe-hydroxides, the electron diffraction pattern shows the superposition of the smectite and the Fe-hydroxides patterns. Fe-hydroxides pattern is compatible with crystal structure characteristics of goethite.

As reported in previous studies (Amouric and Olives 1998; Cuadros et al. 2009), it is difficult to obtain lattice-fringe HR-TEM images from very hydrated clays, as smectites, because of the structural damage caused by the electron beam. Another problem is related to the vacuum of the TEM environment and/or electron irradiation, which cause dehydratation and collapse of smectite. It results that the usually measured smectite spacing is 10 Å in the case of a complete collapse, or >10 Å in case of an incomplete collapse.

At high resolution, the samples generally show smectite packets with lattice fringes whose spacing ranges from 10 to 11 Å (Fig. 5a), but notable differences have been also revealed. For example, Figure 5b presents lattice fringes, which show random interstratification of smectite and mica with measured spacing of 20 Å. This random smectite/mica interstratification has been recognized by the electron diffraction pattern, where it was possible to measure a non-rational order of very diffuse basal reflections with calculated spacing of 11.2 Å, from the (001) spot, 9.8 and 8.9 Å from (002), and 9.8 Å as of (003). Moreover, the EDX spectra of these areas showed an intermediate composition between those usually found for sauconite and mica. In the same figure (Fig. 5b) a fringe spacing of 18 Å was also measured. Somewhere smectite packets presenting alternating fringes at 13 and 10 Å were detected (Fig. 5c). In a two-dimensional lattice image (Fig. 5d) of a smectite packet characterized by lattice fringes with spacing of 11.6 Å, it is possible to recognize crystallographic coherence from layer to layer and that the 11.6 Å spacing is the sum of 4+7.6 Å. The spacing in the perpendicular direction is 4.5 Å, which corresponds to **b**/2. Figure 5e presents a smectite packet with lattice fringe spacing varying between 16 and 17 Å, and wavy microfabric. In the wavy microfabric it is possible to see coalescing and lens-like shaped sauconite packets. Other compact sauconite packets with lattice-fringe spacing of 13–15 Å and wavy microtexture, which is reflected in the curved and lens-like structure of the sauconite layers/packets, can also be recognized in the YA-B sample. Smectite layers also exhibit layer terminations. Iron hydroxide (goethite) and oxide (hematite) associated with smectite have a mosaic-domain type texture (Fig. 5f), in which the different domains present variable orientation and spacing.

It was possible to carry out qualitative chemical analyses (EDX spectra) of particles during the observation, with the Titan TEM used for the textural analysis. In this way, together with textural information, it was possible to obtain data on crystal structure and chemistry of phases (STEM-EDX). It was revealed that in both CCP and PCA, smectite occurs in the two species, sauconite, and beidellite, identified in the Titan by their qualitative chemical differences (Fig. 6). In fact, the Zn and Al contents of the two kinds of smectites are so different that qualitative differentiation is straightforward.

Chemical composition of Zn-clays by TEM-AEM

Considering that AEM is not an absolute-composition technique, and allows determining only the ratios between the various elements, it is usually required to normalize the obtained chemical compositions to the basic formula of the investigated minerals.

From the analyses of the dispersed mineral grains in the samples, it was ascertained that Yanque smectite is mostly composed by sauconite; it is associated with a discrete amount of Zn-bearing beidellite and few grains of illite. Beidellite was detected in all the Yanque samples, but only in YA-A, YA-B, and YA-E proper contamination-free quantitative chemical compositions could be obtained.

In the Accha sample, similarly to Yanque, sauconite is the most abundant clay mineral. Few beidellite and/or montmorillonite grains were also detected, but here they were found intimately associated with sauconite. Consequently, as in some Yanque
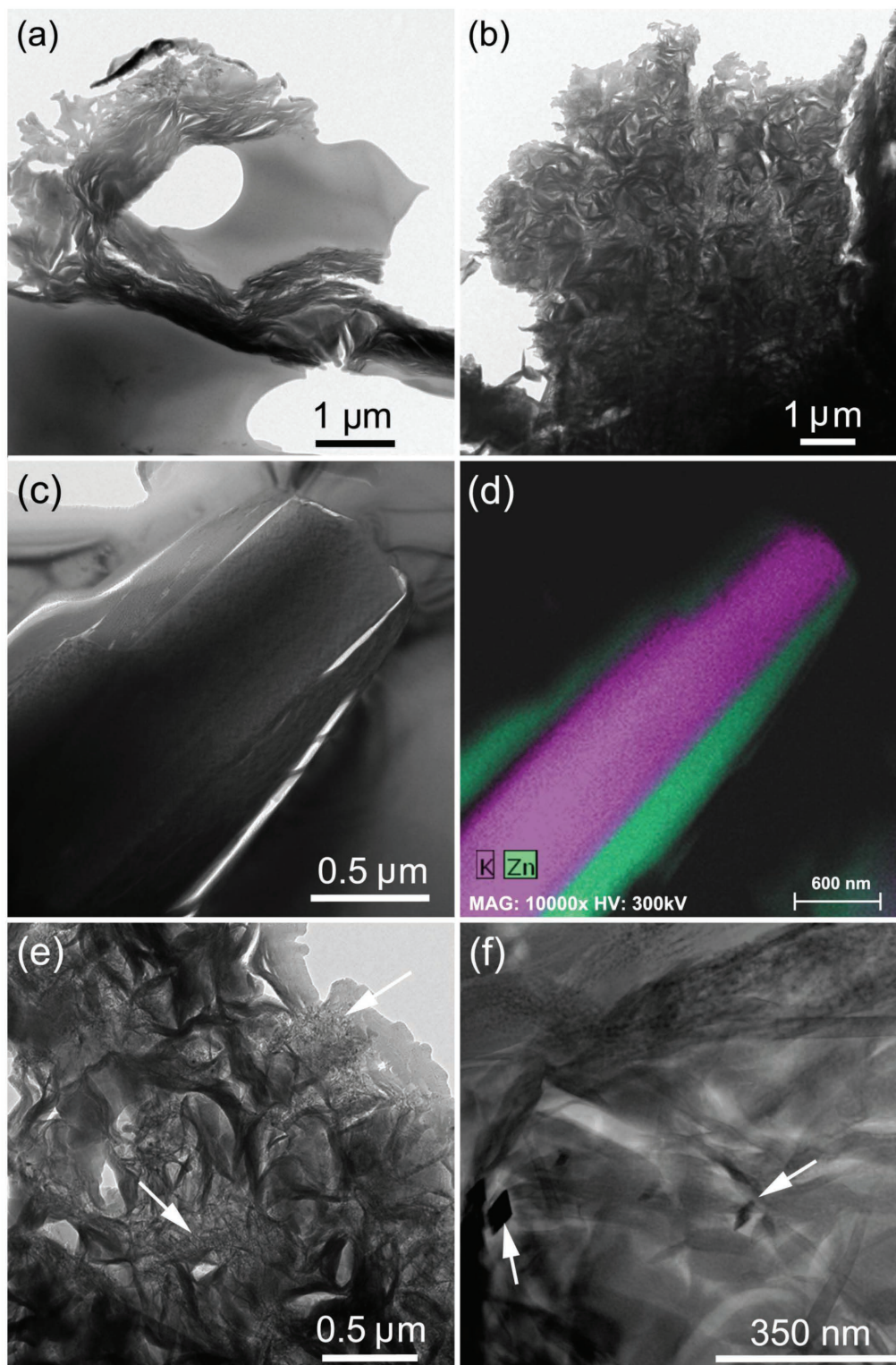
FIGURE 2. (a) Compact clay packages (Sample YA-B). The gray part is the organic resin used to consolidate the sample before the preparation of the thin section. **(b)** Porous clay aggregates (Sample YA-B). **(c and d)** Smectite grains overgrown upon mica nuclei, forming a compact clay package (sample YA-D). By STEM-EDX spectrum, mica contains K as main interlayer cation, and Al as main occupant of the octahedral site. **(e)** Spongy Fe-hydroxides (white arrow) in a porous clay aggregate (Sample YA-B). **(f)** Rhombic Fe-hydroxides micro-grains (white arrows) in a porous clay aggregate (Sample YA-D).
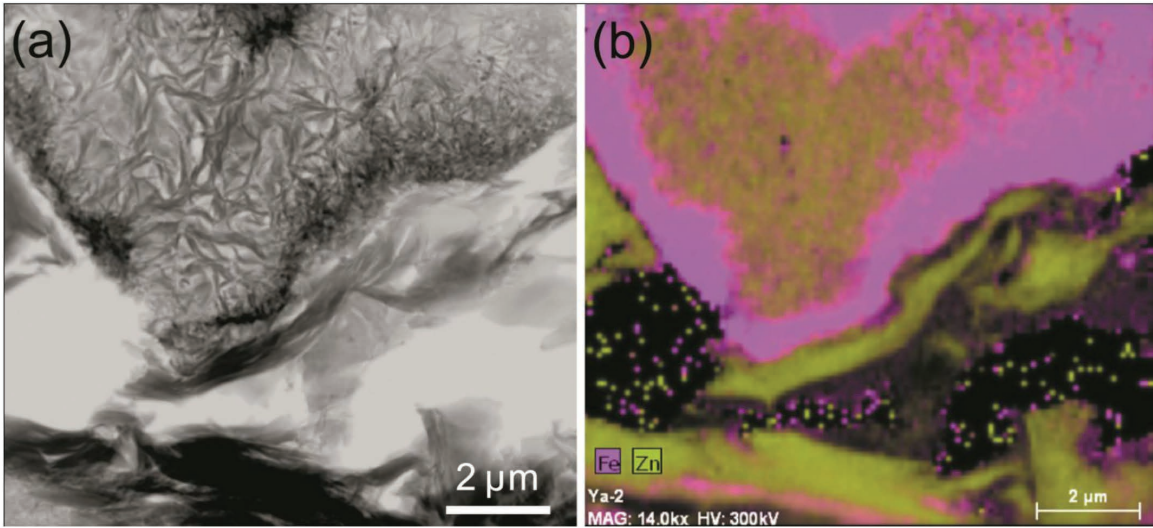
FIGURE 3. (a and **b)** HAADF image and chemical map of sample YA-B: Fe-hydroxides grew filling pores and covering PCA-type smectites.

samples, it was not possible to obtain acceptable contamination-free quantitative chemical composition of this beidellite; however a montmorillonite grain could be analyzed.

In Tables 3 and 4, we report some representative chemical compositions of Zn-clays from the Yanque and Accha samples, normalized to $O_{10}(OH)_2$. The octahedral sites are occupied by Zn, Mg, Mn, Fe, and Al cations, whereas K and Ca were considered as interlayer cations.

Sauconite is characterized by a variable composition (Table 3), which could be, in a minor extent, a consequence of the minor presence of interstratifications with mica layers as shown in Figure 5b. Silicon can fully occupy the tetrahedral site or decrease continuously up to 3.27 atoms per formula unit (apfu) (Fig. 7a), with the remaining amount compensated by Al^{IV} (Fig. 7b). The comparison between Accha and Yanque samples shows that Accha sauconite seems to be characterized by an Al^{IV} amount

$(0.5 < Al^{IV} < 0.8$ apfu) higher than Yanque one $(0.1 < Al^{IV} < 0.7$ apfu) (Fig. 7b).

In both the Accha and Yanque samples, sauconite octahedral composition remains coherent through the data (Figs. 7 and 8). Most of the octahedral site is occupied by Zn, which has been found to completely fill the site only in one case (3 apfu) (Fig. 7c); it generally varies continuously between 2.66 apfu and 1.67 apfu, and only in three grains comes down to 1.40 apfu. The octahedral site can be also occupied by Al (0.13–0.72 apfu) (Fig. 7c), Mg (up to 0.46 apfu, generally lower than 0.30 apfu) (Fig. 7d), Fe (up to 0.57 apfu, generally below 0.40 apfu) (Fig. 7e), and Mn (between 0.04 and 0.48 apfu in a few grains, but generally below detection limits). As regards the measured octahedral Fe, sauconite is often intergrown with Fe-hydroxides and oxides: consequently the iron content could be enhanced by the contribution of oxyhydroxides-related Fe in some analytical points.
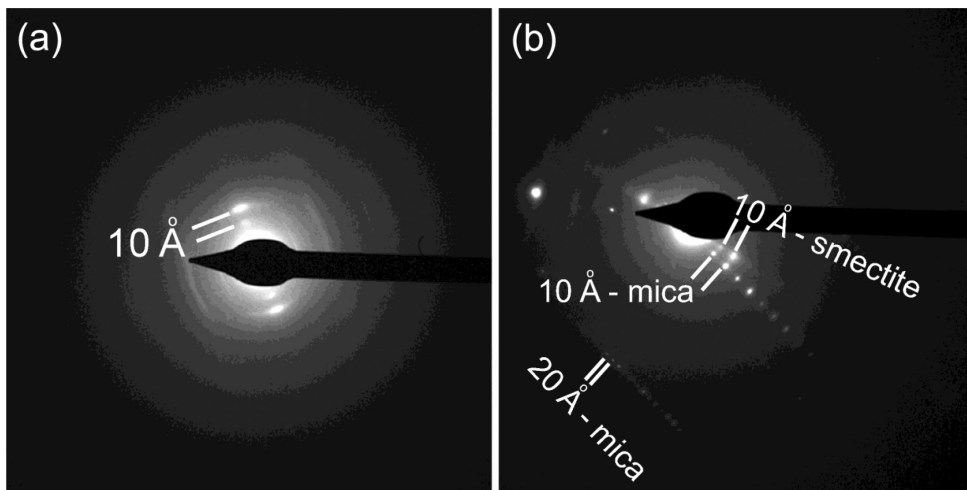

FIGURE 4. (a) Electron diffraction pattern of a compact smectite packet (Sample YA-B). **(b)** Electron diffraction pattern of the smectite packet epitaxial over a mica grain shown in Figures 2c and 2d (Sample YA-D).
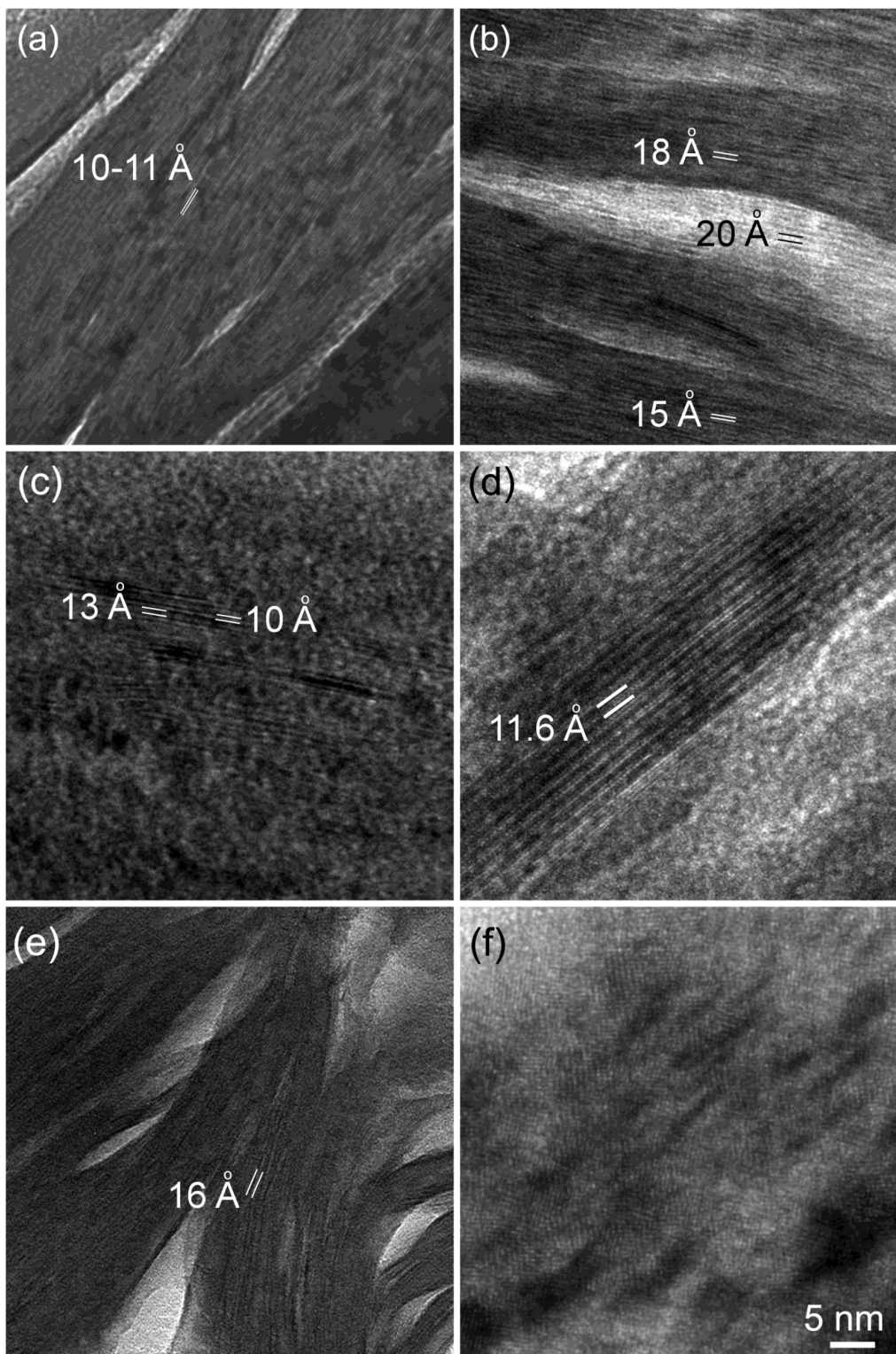
FIGURE 5. Sample YA-D. (**a**) Close up view of Figure 2c: sauconite packets with lattice fringes spacing of 10–11 Å. (**b**) Smectitic packets together with other that shows a random interstratification of smectite and mica with measured spacing of 20 Å and intermediate composition between those of smectite and mica. (**c**) Smectite packet with alternating fringes at 13 and 10 Å. Sample YA-B. (**d**) Compact smectite packet showing a two-dimensional fringe spacing of 11.6 and 4.5 Å. (**e**) Compact smectite packet with lattice fringe spacing variable between 16 and 17 Å and wavy microfabric. (**f**) Hematite associated with sauconite, showing mosaic-domain type texture.
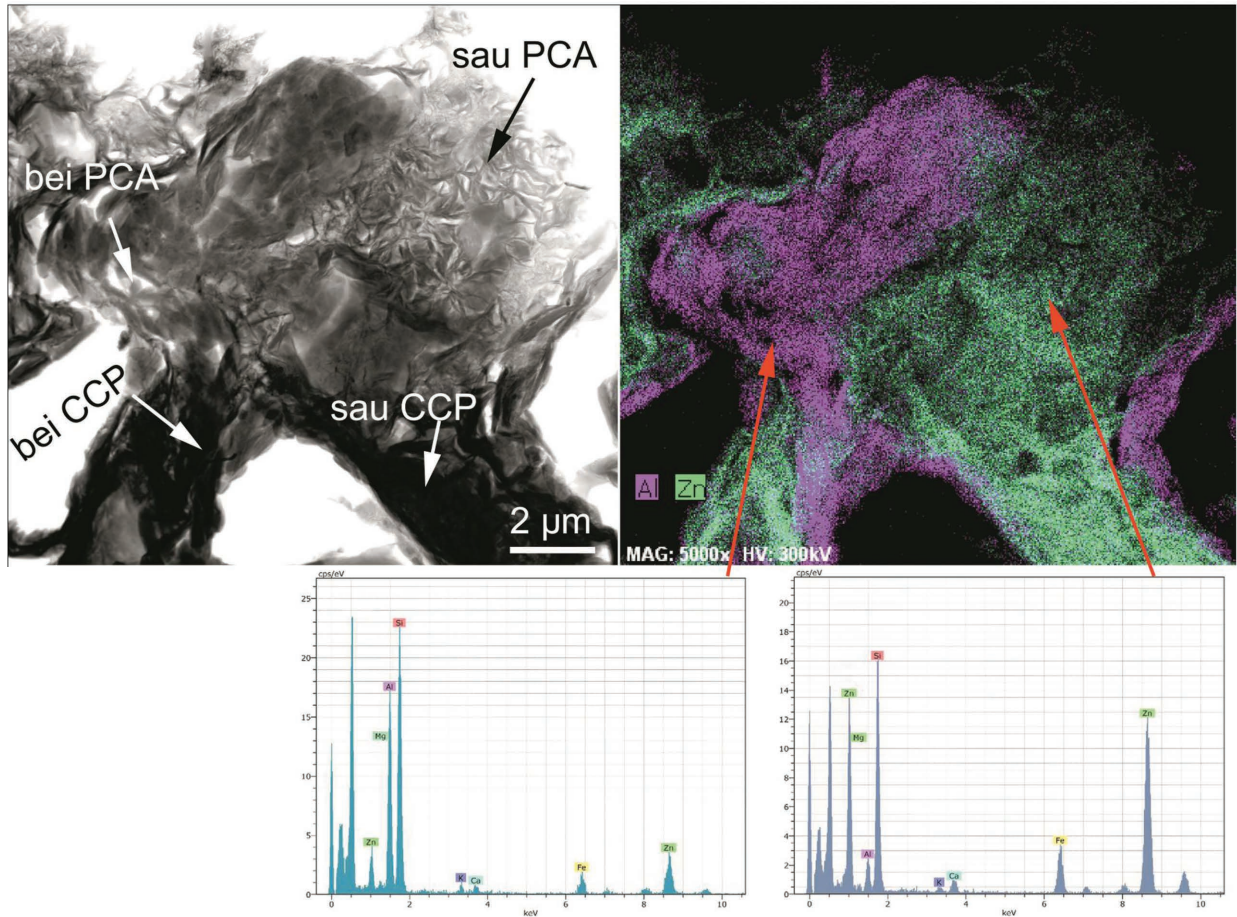
FIGURE 6. HAADF image and chemical map (Zn and Al) of sample YA-B: sauconite (green) and beidellite (purple) compact clay packages and porous clay aggregates. The qualitative EDX sauconite spectrum is characterized by a Zn peak more intense than in the beidellite spectrum, instead characterized by a more intense Al peak.

Plotting Zn/Al_{tot} vs. Si/Al_{tot} a positive correlation is observed, with ratio values ranging from 1 to 5 for Zn/Al_{tot} and from 2 to 10 for Si/Al_{tot} (Fig. 7f).

The interlayer content is represented by K and Ca occurring in variable amounts, within the ranges of 0.00–0.27 apfu and 0.00–0.38 apfu for K and Ca, respectively (Figs. 7g and 7h). Calcium is more abundant than K, with the values of the latter generally approaching zero. K and Ca are positively correlated (Fig. 7h), and Ca/K ratio ranges between 1 and 8. The Accha

sauconite contains Ca amounts slightly higher than Yanque sauconite, as a result of the charge compensation related to the different Al^{IV} content (Figs. 7b and 7h). As previously discussed, Na cannot be revealed in the presence of Zn by TEM-AEM, and hence has not considered as interlayer cation.

Correlation of Zn/Al_{tot} vs. Ca/K ratios generally show a positive trend, which is coherent with charge compensation between the layers (Fig. 7i).

As regards beidellite, the following data are associated with

TABLE 3. Representative structural formulas (apfu) of sauconite from Yanque and Accha deposits

	YA-A	YA-A	YA-B	YA-C	YA-C	YA-D	YA-D	YA-E	ACC	ACC	ACC
Si	3.88	3.64	3.64	3.31	3.65	3.49	3.69	3.54	3.38	3.48	3.23
Al^{IV}	0.12	0.36	0.36	0.69	0.35	0.51	0.31	0.46	0.62	0.52	0.77
Al^{VI}	0.36	0.28	0.33	0.72	0.35	0.20	0.34	0.23	0.27	0.48	0.48
Mg	0.11	0.25	0.24	0.26	0.18	0.22	0.05	0.46	0.15	0.16	0.24
Fe^{2+}	0.13	–	0.15	0.31	0.04	0.18	0.18	0.13	0.20	–	0.09
Zn	1.97	2.34	2.29	1.43	2.18	2.37	2.24	2.08	2.28	2.07	2.02
Mn	0.18	0.00	–	0.02	0.04	–	–	–	–		
Σ	2.75	2.87	3.01	2.74	2.78	2.97	2.82	2.89	2.90	2.71	2.84
K	0.05	0.05	0.09	0.27	0.07	0.07	0.07	0.05	0.04	0.18	–
Ca	0.11	0.14	0.21	0.11	0.18	0.15	0.13	0.20	0.26	0.22	0.31
Σ charge	0.27	0.34	0.51	0.49	0.43	0.37	0.33	0.46	0.55	0.62	0.62

Note: Calculated on the basis of 12 total anions, $O_{10}(OH)_2$.

TABLE 4. Representative structural formulas (apfu) of beidellite from the Yanque deposit

	YA-A	YA-B	YA-B		YA-E	YA-E
Si	3.51	3.83	3.37	Si	3.62	3.37
Al^{IV}	0.49	0.17	0.63	Al^{IV}	0.38	0.63
Al^{VI}	1.65	1.49	1.46	Al^{VI}	2.00	2.01
Mg	0.14	0.14	–	Mg	–	
Fe^{3+}	0.17	0.29	0.26	Fe^{3+}	0.03	0.03
Zn	0.33	0.14	0.52	Zn	0.03	0.05
Mn	0.02	–	–	Mn	–	–
Σ	2.31	2.06	2.24	Σ	2.07	2.10
Na	–	–	–	Mg	0.09	0.12
K	0.05	0.16	0.14	K	0.02	0.03
Ca	–	0.05	0.14	Ca	–	0.05
Σ charge	0.05	0.26	0.42	Σ charge	0.19	0.38

Note: Calculated on the basis of on 12 total anions, $O_{10}(OH)_2$.

Yanque samples: beidellite was detected by AEM analysis in few areas (Table 4), and shows a tetrahedral occupancy very similar to sauconite, with Si in the range of 3.36–3.83 apfu (Fig. 7a). The octahedral Al generally varies between 1.29 apfu and the maximum stoichiometric value of 2 apfu (measured only in two grains). In the Zn-bearing beidellites, Zn varies between 0.14 and 0.54 apfu (Fig. 7c). As in sauconite, the other octahedral cations show low values: Mg varies between 0.00–0.31 apfu (Fig. 7d), Fe ranges between 0.00–0.38 apfu (Fig. 7e), whereas Mn is lacking, except for 0.02 apfu detected only in one Zn-beidellite grain. The Zn/Al_{tot} and Si/Al_{tot} ratios vary for a very short range

of values (Zn/Al_{tot} between 0–0.25; Si/Al^{tot} between 1.27–2.31) and no correlations were observed (Fig. 7f). Zn vs. Al^{VI} plot (Fig. 7c) shows that the distribution of the two elements is clearly related to their charge, with divalent Zn reaching a maximum occupancy of 3 apfu in sauconite, whereas trivalent Al reaches a maximum occupancy of 2 apfu in beidellite.

In dioctahedral clay minerals, the interlayer cations are K and Ca, as already discussed for sauconite, but in beidellite K (max. 0.17 apfu) is prevailing compared to Ca (max. 0.14 apfu) (Fig. 7h). The K and Ca contents are positively correlated, but the Ca/K statistic ratio is around 1.2, with absolute ratios ranging between 0 and 1.5 (Fig. 7h). This correlation, more favorable to K than Ca is in agreement with the charge compensation principle and the higher Al^{3+} content in beidellite than in sauconite. Smectites can have some Mg amounts in the interlayer; however, no definitive criteria exist on Mg distribution between the octahedral sheet and the interlayer. Some formulas showing high-octahedral and/or low-interlayer sums could be better adjusted considering part of Mg as an interlayer cation, which could explain such anomalies. Nevertheless, we have accepted such possibility only for straightforward cases as those of the beidellites in sample YA-E (Table 4).

The other detected clays also show discrete Zn contents. Montmorillonite is characterized by an octahedral occupancy almost equally subdivided between Al and Mg-Zn, which have amounts of 1.06 apfu Al, 0.55 apfu Mg, and 0.39 apfu Zn. An
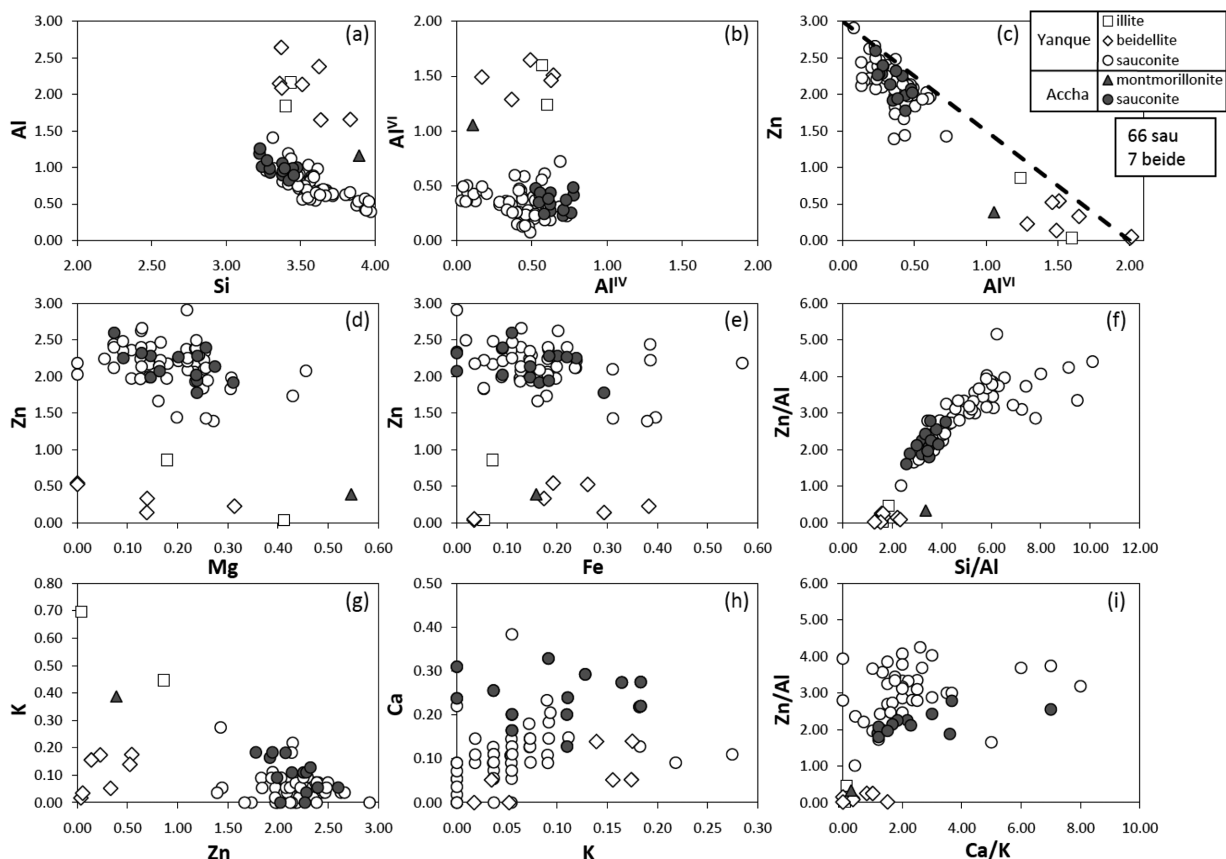

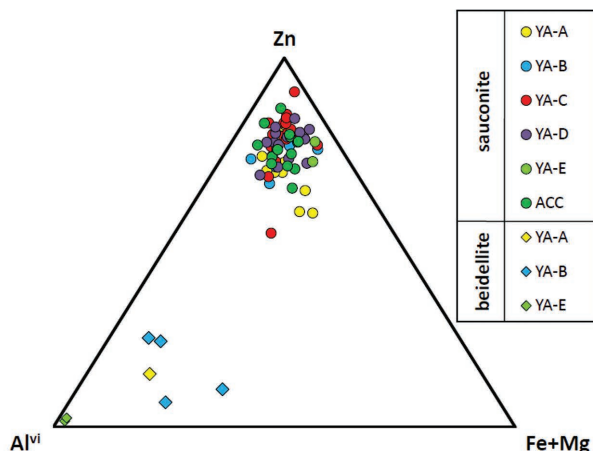**FIGURE 7.** Chemical compositions of clays from the Yanque and Accha deposits.

FIGURE 8. Octahedral chemical compositions of sauconite and beidellite on the Zn-Al^{VI}-Fe+Mg diagram.

illite grain with interlayer cationic content of ~0.55 apfu is characterized by 0.04 apfu Zn in the octahedral site. Chemical analysis of micas was not considered to be an objective during AEM data acquisition; hence the micas were not systematically analyzed. However, several micas completely free of Zn were found during the HRTEM analysis (e.g., see Figs. 2c and 2d), together with others with a minor Zn content.

DISCUSSION

This TEM-HRTEM study carried out on natural Zn-smectites allowed to obtain new results mainly focused on the very detailed identification of the clay type, on the mineral texture, and chemical composition.

Clay type identification

Our results have shown that the Zn-bearing clay fraction of the Accha and Yanque supergene ores, previously simply identified as sauconite (Accha) or sauconite+Zn-bearing illite+kaolinite (Yanque), is indeed a mixture of several smectites, i.e., the trioctahedral sauconite and the dioctahedral (both Zn-bearing and Zn-poor) beidellite. The occurrence of a Zn-bearing beidellite seems to have been never ascertained, either in nonsulfide Zn deposits or worldwide.

In our opinion, the misinterpretation of the nature of the clay minerals, made in the previous studies is due to the use of protocols of combined XRD and EPMA, routinely applied to the mineralogical evaluation of the ores, on the basis of the previous literature on this type of deposits. Specifically, bulk-rock XRD analyses allowed to basically identifying the occurrence of smectite in the Accha deposit, and of smectite, mica (illite), and kaolinite in the Yanque deposit. When a combination of microbeam analyses as EPMA-EDS was employed, the numerous textural and petrographic observations led to automatically consider all the Zn-Al-Si-H$_2$O analyses as sauconite, the K-Al-Si-H$_2$O-(few Zn) analyses as Zn-bearing illite, and Al-Si-H$_2$O-(few Zn) analyses as Zn-bearing kaolinite. The TEM-STEM-HRTEM technique enabled instead to test every chemical STEM analysis, by using electron diffraction and lattice images, and allowed to confirm in the studied samples the occurrence of sauconite and of a Zn-bearing mica

(not deeply investigated in this study). It also evidenced that the analyses containing Al-Si-H$_2$O-(few Zn) were not corresponding to a Zn-bearing kaolinite, but again to a smectite and specifically to a Zn-bearing beidellite. In our opinion, the rare use of TEM-STEM when studying natural Zn-clays (except the pioneer STEM study of Steinberg et al. 1985), could have hampered a correct identification of other types of Zn-smectite in several ore deposits.

Texture of minerals

In the texture here called CCP, smectite frequently overgrows the mica grains. The overgrowing of CCP smectite upon mica nuclei probably indicates that the CCP inherit the crystallographic orientation from previous phyllosilicates, which could act as templates. This is also supported by the presence of the random interstratification of smectite and mica, which has been recognized by the intermediate chemical composition, by lattice fringe images where packets showing 20 Å spacing were directly observed, and by the electron diffraction pattern. In the latter, it was possible to measure a non-rational order of basal reflections with calculated spacing of 11.2 to 8.9 Å.

Direct HRTEM observation of lattice fringes of the compact sauconite packets often showed a variable spacing, generally ranging around 10–11 Å, but also varying up to 13, 15, or 18 Å. We interpret these variable thicknesses of the smectite layers as possibly related to a different contracting behavior (related to TEM vacuum) of layers, in correspondence to different types of interlayer cation content (Nieto et al. 1996). An alternative explanation (especially for the 18 Å spacing) could be an interstratification, however not precisely identified during this study.

The occurrence in the CCP of coalescing packets, lens-like shaped packets, wavy microtexture, and layer terminations are features similar to those observed in other smectites of various origins (e.g., Mellini et al. 1991; Nieto et al. 1996; Vazquez et al. 2014).

The PCA textures are typical of clays directly precipitated from solutions. Consequently, they are constituted by newly formed smectite grown in the cavities existing between the CCP. Spongy or rhombic goethite and hematite occur in the PCA porosity (Fig. 3). This common textural relationship suggests that the Fe-hydroxides and oxides are syn- to post-genetic with the precipitations of clays.

Like CCP, PCA show an annular electron diffraction pattern that indicates a turbostratic disorder, typical of most smectites.

From a textural point of view, there is no difference between sauconite and beidellite, suggesting a syn-genetic origin.

Chemical composition

This first TEM-AEM investigation demonstrates that the chemical composition of sauconite varies in a range of values, without any chemical gap, around the average composition:

$$Ca_{0.15}K_{0.05}(Zn_{2.1}Mg_{0.2}Al_{0.4}Fe_{0.15}Mn_{0.02})(Si_{3.5}Al_{0.5})O_{10}(OH)_2 \cdot nH_2O.$$

As expected, sauconite has been found to have a chemical composition characterized by Zn associated with Mg, Al, Fe, and Mn in the octahedral layer, a variable but significant Al tetrahedral occupancy, and Ca and K as major interlayer cations.

The wide range of measured compositions could partially be affected also by smectite/mica interstratification, clearly observed in the Yanque samples. This can likely influence Al^{IV}, Mg, and interlayer cation contents, and led them to vary more

than expected for such type of smectite.

The only sauconite sample from Accha analyzed here shows a composition characterized by an average Al^{IV} content slightly higher than in the above mentioned formula ($Al^{IV} \sim 0.65$ apfu), and as consequence of the charges compensation, also by a slightly higher interlayer Ca content (Ca ~ 0.22–0.23 apfu). Anyway, it is reasonable to suppose that this chemical feature related to just one sample could not be fully representative of the whole deposit.

Another remarkable result of this research is that beidellite from both these Peruvian nonsulfide deposits is always characterized by variable but significant Zn contents in its structure. Unfortunately, the analysis of beidellites in the Accha sample has not produced acceptable results, and only data from Yanque samples could be presented.

Beidellites have an average composition close to stoichiometry with the addition of Zn:

$$Ca_{0.05}K_{0.15}(Al_{1.6}Zn_{0.25}Mg_{0.1}Fe_{0.15})(Si_{3.6}Al_{0.4})O_{10}(OH)_2 \cdot nH_2O.$$
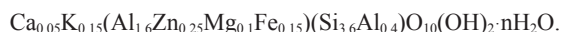
There are various studies on beidellite containing divalent cations, and on its chemical relationship with trivalent smectite end-members, e.g., saponite (Grauby et al. 1993, and references therein). They showed that the natural trioctahedral-dioctahedral smectite series is discontinuous with large chemical gaps. From our data, a chemical gap also exists between sauconite and Zn-bearing beidellite, with an effective maximum Al content in sauconite around 0.50 apfu and a minimum content in beidellite around 1.30 apfu.

The Zn/Al_{tot} vs. Si/Al_{tot} positive correlation registered for sauconite, against the very short range of values of the same ratios of beidellites, demonstrates that the relative sauconite composition is more variable than beidellite composition in the studied samples. A consequence of the variable amount of Zn-Al in the octahedral site of sauconite and beidellite is that also the interlayer cations distribution within the clay lattice, being strictly dependent on the charge balance, vary accordingly.

IMPLICATIONS

The mineralogical study of clay minerals from Accha and Yanque nonsulfide deposits demonstrates that the mineral compounds, up to now usually called "sauconites," indeed correspond to a mixture of sauconite and Zn-bearing beidellite. This is a relevant hint, demonstrating that in such Zn-bearing systems both trioctahedral and dioctahedral smectitic structures can form, as commonly observed in Zn-free natural paragenesis of trioctahedral and dioctahedral smectites, like saponite and beidellite (e.g., Abad et al. 2003; Jiménez-Millán et al. 2008). In low-temperature environments, newly formed phases are highly dependent on the local chemistry; hence the chemical nature of each smectite grain is strongly controlled by the near particles and fluids from which it has grown (e.g., Drief et al. 2001)

The textures of the clays suggest two genetic mechanisms, i.e., smectites can grow on previous phyllosilicates (mica) (CCP texture), and/or directly precipitate from solutions (PCA texture). The first texture confirms what reported in previous studies by Boni et al. (2009) and Mondillo et al. (2014a), when the authors refer to sauconite as a "wall-rock replacement" mineral. The

second PCA texture, instead, likely opens new genetic scenarios, because, as reported in literature (Roy and Mumpton 1956; Tiller and Pickering 1974; Harder 1977; Kloprogge et al. 1999; Higashi et al. 2002; Petit et al. 2008; Pascua et al. 2010), experimental studies demonstrated that sauconite can precipitate from solutions of silicic acid, variously mixed with Zn and other components, at temperatures ranging between 20 and 200 °C for pH of 6 to 12. Consequently, it is possible to admit that PCA smectite can also form during hydrothermal processes. Considering the geological features of the deposits, their strong association with oxidized sulfides, and the link between PCA and Fe-hydroxides and oxides (typical of gossans and of weathering-related environments), we can affirm beyond doubt that most of the smectite is genetically related to supergene processes. However, at least part of it could have also been precipitated through the hydrothermal fluid circulation, which was active in the area during sulfides mineralization or slightly after their deposition, before the formation of the Fe-hydroxides and oxides typical of the gossan.

The discovery in the Peruvian nonsulfide Zn deposits of a natural association of smectites belonging to the trioctahedral sauconite and the dioctahedral (both Zn-bearing and Zn-poor) beidellite types should be considered not only a simple new mineral finding, but also an important methodological clue for future mineralogical evaluation of Zn-nonsulfide deposits with possible processing implications.

REFERENCES CITED

Abad, I., Jimenez-Millan, J., Molina, J.M., Nieto, F., and Vera, J.A. (2003) Anomalous reverse zoning of saponite and corrensite caused by contact metamorphism and hydrothermal alteration of marly rocks associated with subvolcanic bodies. Clays and Clay Minerals, 51, 543–554.

Ahn, H.I. (2010) Mineralogy and geochemistry of the non-sulfide Zn deposits in the Sierra Mojada district, Coahuila, Mexico, 193 p. Ph.D. thesis, University of Texas, Austin.

Amouric, M., and Olives, J. (1998) Transformation mechanisms and interstratification in conversion of smectite to kaolinite: an HRTEM study. Clays and Clay Minerals, 46, 521–527.

Balassone, G., Rossi, M., Boni, M., Stanley, G., and McDermott, P. (2008) Mineralogical and geochemical characterization of nonsulfide Zn-Pb mineralization at Silvermines and Galmoy (Irish Midlands). Ore Geology Reviews, 33, 168–186.

Boland, M.B., Kelly, J.G., and Schaffalitzky, C. (2003) The Shaimerden supergene zinc deposit, Kazakhstan: a preliminary examination. Economic Geology, 98, 787–795.

Boni, M. (2005) The geology and mineralogy of nonsulfide zinc ore deposits. Proceedings of LEAD and ZINC '05 Congress, Kyoto, Japan, 17–19 October 2005, 15 p.

Boni, M., Balassone, G., Arseneau, V., and Schmidt, P. (2009) The nonsulphide zinc deposit at Accha (southern Peru): geological and mineralogical characterization. Economic Geology, 104, 267–289.

Borg, G., Kärner, K., Buxton, M., Armstrong, R., and Van Der Merwe, S.W. (2003) Geology of the Skorpion supergene zinc deposit, southern Namibia. Economic Geology, 98, 749–771.

Cesàro, G. (1927) Sur la fraipontite, silicate basique hydraté de zinc et d'aluminum. Annales Societe Geologique Belgique, 50, 106–110.

Cliff, G., and Lorimer, G.W. (1975) The quantitative analysis of thin specimens. Journal of Microscopy, 103, 203–207.

Coppola, V., Boni, M., Gilg, H.A., Balassone, G., and Dejonghe, L. (2008) The "calamine" nonsulfide Zn–Pb deposits of Belgium: Petrographical, mineralogical and geochemical characterization. Ore Geology Reviews, 33, 187–210.

Cuadros, J., Nieto, F., and Wing-Dudek, T. (2009) Crystal-chemical changes of mixed-layer kaolinite-smectite with progressive kaolinization, as investigated by TEM-AEM and HRTEM. Clays and Clay Minerals, 57, 742–750.

Drief, A., Nieto, F., and Sánchez-Navas, A. (2001) Experimental clay-mineral formation from a subvolcanic rock by interaction with 1 M NaOH solution at room temperature. Clays and Clay Minerals, 49, 92–106.

Emselle, N., McPhail, D.C., and Welch, S.A. (2005) Reliance, Flinders Ranges. In I.C. Roach, Ed., Mineralogy, Geochemistry and Zinc Dispersion around a Nonsulfide Orebody, Regolith 2005—Ten Years of CRC LEME, 86–90.

Faust, G.T. (1951) Thermal analysis and X-ray studies of sauconite and of some zinc minerals of the same paragenetic association. American Mineralogist, 36, 795–822.

Fransolet, A.M., and Bourguignon, P. (1975) Données nouvelles sur la fraipontite de Moresnet (Belgique). Bulletin de la Société Française de Minéralogie, 98, 235–244.

Frondel, C. (1972) The Minerals of Franklin and Sterling Hill—a checklist, 94 p. Wiley Interscience, New York.

Genth, F.A. (1875) Mineralogy of Pennsylvania. Second Geological Survey of Pennsylvania, 120 p.

Grauby, O., Petit, S., Decarreau, A., Baronnet, A. (1993) The beidellite-saponite series: an experimental approach. European Journal of Mineralogy, 5, 623–635.

Gu, X., and Evans, J. (2008) Surface complexation modeling of Cd(II), Cu(II), Ni(II), Pb(II) and Zn(II) adsorption onto kaolinite. Geochimica et Cosmochimica Acta, 72, 267–276.

Güven N. (1988) Smectite. In S.W. Bailey, Ed., Hydrous Phyllosilicates, 19, p. 497–559. Reviews in Mineralogy, Mineralogical Society of America, Chantilly, Virginia.

Harder, H. (1977) Clay mineral formation under lateritic weathering conditions. Clay Minerals, 12, 281–288.

Heaney, P.J., Post, J.E., and Evans, H.T. (1992) The crystal structure of bannisterite. Clays and Clay Minerals, 40, 129–144.

Higashi, S., Miki, K., and Komarneni, S. (2002) Hydrothermal synthesis of Zn-smectite. Clays and Clay Minerals, 50, 299–305.

Hitzman, M.W., Reynolds, N.A., Sangster, D.F., Allen, C.R., and Carman, C.E. (2003) Classification, genesis, and exploration guides for nonsulfide zinc deposits. Economic Geology, 98, 685–714.

Jiménez-Millán, J., Abad, I., and Nieto, F. (2008) Contrasting alteration processes in hydrothermally altered dolerites from the Betic Cordillera, Spain. Clay Minerals, 43, 267–280.

Kärner, K. (2006) The metallogenesis of the Skorpion non sulphide zinc deposit, Namibia, 133 p. Ph.D. thesis (Dr. rer. nat.), Mathematisch-naturwissenschaft-lich-technischen Fakultät der Martin-Luther-Universität Halle-Wittenberg, Germany.

Kloprogge, T., Komarneni, S., and Amonette, J. (1999) Synthesis of smectite clay minerals: a critical review. Clays and Clay Minerals, 47, 529–554.

Large, D. (2001) The geology of non-sulphide zinc deposits—an overview. Erzmetall, 54, 264–276.

Mellini, M., Nieto, F., Alvarez, F., and Gómez-Pugnaire, M.T. (1991) Mica-chlorite intermixing and altered chlorite from the Nevado-Filabride micaschists, Southern Spain. European Journal of Mineralogy, 3, 27–38.

Miranda-Trevino, J.C., and Coles, A.C. (2003) Kaolinite properties, structures and influence of metal retention on pH. Applied Clay Science, 23, 133–139.

Mondillo, N., Boni, M., Balassone, G., and Villa, I.M. (2014a) The Yanque Prospect (Peru): form polymetallic Zn-Pb mineralization to a nonsulfide deposit. Economic Geology, 109, 1735–1762.

Mondillo N., Boni M., Balassone G., and Villa I.G. (2014b) Polymetallic Zn-Pb mineralization in the Cuzco area (Peru): Lead isotope geochemistry Accha-Larisa district. Mineral Deposits Studies Group Conference, Southampton, U.K., 16–19 December 2014.

Newman, A.C.D., and Brown, G. (1987) The chemical constitution of clays. In A.C.D. Newman, Ed., Chemistry of Clays and Clay Minerals, Mineralogical Society Monograph, 6, p. 1–128, Wiley Interscience, New York.

Nieto, F., and Livi, K.J.T. (2013) Minerals at the nanoscale. EMU Notes in Mineralogy, 14, 440 p.

Nieto, F., Ortega-Huertas, M., Peacor, D., and Arostegui, J. (1996) Evolution of illite/smectite from early diagenesis through incipient metamorphism in sediments of the Basque-Cantabrian Basin. Clays and Clay Minerals, 44, 304–323.

Pascua, C.S., Ohnuma, M., Matsushita, Y., Tamura, K., Yamada, H., Cuadros, J., and Ye, J. (2010) Synthesis of monodisperse Zn-smectite. Applied Clay Science, 48, 55–59.

Peacor, D.R., Rouse, R.C., and Bailey, S.W. (1988) Crystal structure of franklin-furnaceite: a tri-dioctahedral zincosilicate intermediate between chlorite and mica. American Mineralogist, 73, 876–887.

Pecho, V., and Blanco, E.Z. (1983) Geología de los cuadrángulos de Chalhuanca, Antabamba y Santo Tomás: Instituto de Geología, Minería y Metalurgia, Boletín, Lima, Peru, n. 35, 97 p.

Perelló, J., Carlotto, V., Zárate, A., Ramos, P., Posso, H., Neyra, C., Caballero, A., Fuster, N., and Muhr, R. (2003) Porphyry-style alteration and mineralization of the Middle Eocene to Early Oligocene Andauaylas-Yauri belt, Cuzco region, Peru. Economic Geology, 98, 1575–1605.

Petit, S., Righi, D., and Decarreau, A. (2008) Transformation of synthetic Zn-stevensite to Zn-talc induced by the Hofmann-Klemen effect. Clays and Clay Minerals, 56, 645–654.

Robert, J.L., and Gaspérin, M. (1985) Crystal structure refinement of hendricksite, a Zn- and Mn-rich trioctahedral potassium mica: a contribution to the crystal chemistry of zinc-bearing minerals. TMPM Tschermaks Mineralogische und Petrographische Mitteilungen, 34, 1–14.

Ross, C.S. (1946) Sauconite—a clay mineral of the montmorillonite group. American Mineralogist, 31, 411–424.

Roy, D.M., and Mumpton, F.A. (1956) Stability of minerals in the system ZnO-SiO$_2$-H$_2$O. Economic Geology, 51, 432–443.

Rule, A.C., and Radke, F. (1988) Baileychlore, the Zn end member of the triocta-hedral chlorite series. American Mineralogist, 73, 135–139.

Srivastava, P., Singh, B., and Angove, M. (2005) Competitive adsorption behavior of heavy metals on kaolinite. Journal of Colloid and Interface Science, 290, 28–38.

Steinberg, M., Rautureau, M., and Rivière, M. (1985) Analysis of zinciferous clays from central Tunisia using a scanning transmission electron microscope (STEM). Chemical Geology, 48, 157–164.

Tiller, K.G., and Pickering, J.G. (1974) The synthesis of zinc silicates at 20°C and atmospheric pressure. Clays and Clay Minerals, 22, 409–416.

Vazquez, M., Nieto, F., Morata, D., Droguett, B., Carrillo-Rosua, F.J., and Morales, S. (2014) Evolution of clay mineral assemblages in the Tinguiririca geothermal field, Andean Cordillera of central Chile: an XRD and HRTEM-AEM study. Journal of Volcanology and Geothermal Research, 282, 43–59.

Will, P., Friedrich, F., Hochleitner, R., and Gilg, H.A. (2014) Fraipontite in the hydrothermally overprinted oxidation zone of the Preguiça mine, Southern Portugal. Abstract Mid-European Clay Conference, 16–19 September 2014, Dresden.

Zincore Metals, Inc. (2013) AZOD Zinc Oxide project, NI 43-101 Technical Report on a Preliminary Feasibility Study: Zincore Metals, Inc., Vancouver, Canada (http://www.zincoremetals.com/_shared/pdf/170848_Zincore_PFS_TechReport_AZOD_26August2013_Final.pdf).